SUPPORTING INFORMATIO

Ultrafast Response UV-Regulated Graphene-Based NO_2 Gas Sensor

Wei Jin[1], Cao Tang[1], Hongyuan Zhao[1], Xue Xiao[1], Xin Qi[1], Xiangting Zhang[1], Hafiza Sana Haider[1], Jianxiong Zhao[1,2,3], Yanqing Ma[1,2,3,4*], Lei Ma[1,2,3*]

[1]Tianjin International Center for Nanoparticles and Nanosystems, Tianjin University, Tianjin, P. R. China, 300072

[2] Tianjin Key Laboratory of Low-dimensional Electronic Materials and Advanced Instrumentation, Tianjin, P. R. China, 300072

[3]Haihe laboratory for low dimensional electronic materials, Tianjin, P.R. China, 300072

[4]School of Precision Instrument and Opto-electronics Engineering, Tianjin University, Tianjin, P. R. China, 300072

*Corresponding authors: E-mail: mayanqing@tju.edu.cn; E-mail: lei.ma@tju.edu.cn

Table S1. Reagents and materials

Reagents and materials	Specification	Supplier	CAS No.
Ethanol	AR	Sinopharm Chemical Reagent Co., Ltd. (China)	64-17-5
Acetone	AR	Sinopharm Chemical Reagent Co., Ltd. (China)	67-64-1
Argon	99.999%	Tianjin Best Gas Co., Ltd. (China)	7440-37-1
Methane	99.999%	Tianjin Best Gas Co., Ltd. (China)	74-82-8
Hydrogen	99.999%	Tianjin Best Gas Co., Ltd. (China)	1333-74-0
Nitrogen	99.999%	Tianjin Best Gas Co., Ltd. (China)	7727-37-9
Oxygen	99.999%	Tianjin Best Gas Co., Ltd. (China)	7782-44-7

Reagents and materials	Specification	Supplier	CAS No.
Potassium persulfate	AR	Tianjin Damao Chemical Reagent Co., Ltd. (China)	7727-21-1
Nitrogen dioxide	100 ppm	Tianjin Boliming Technology Co., Ltd. (China)	10102-44-0
Hydrogen sulfide	5 ppm	Tianjin Boliming Technology Co., Ltd. (China)	7783-06-4
Methane	99.999%	Tianjin Boliming Technology Co., Ltd. (China)	74-82-8
Carbon monoxide	1%	Tianjin Boliming Technology Co., Ltd. (China)	630-08-0
Hydrogen	1000 ppm	Tianjin Boliming Technology Co., Ltd. (China)	1333-74-0
Propane	50%	Tianjin Boliming Technology Co., Ltd. (China)	74-98-6
Ethylene	50%	Tianjin Boliming Technology Co., Ltd. (China)	74-85-1
Ammonia	1%	Tianjin Boliming Technology Co., Ltd. (China)	7664-41-7
Poly (methyl methacrylate)	495A4	MicroChem Corp. (USA)	9011-14-7
Trimethylaluminum	99.999%	Jiaxing KEMICRO Electronic Equipment Co., Ltd. (China)	75-24-1
Sodium hydroxide	97%	Aladdin Biochemical Technology Co., Ltd. (China)	1310-73-2
Gold	99.99%	YipinchuanCheng Co., Ltd. (China)	7440-57-5
Chromium	99.99%	YipinchuanCheng Co., Ltd.	7440-47-3

Reagents and materials	Specification	Supplier	CAS No.
		(China)	

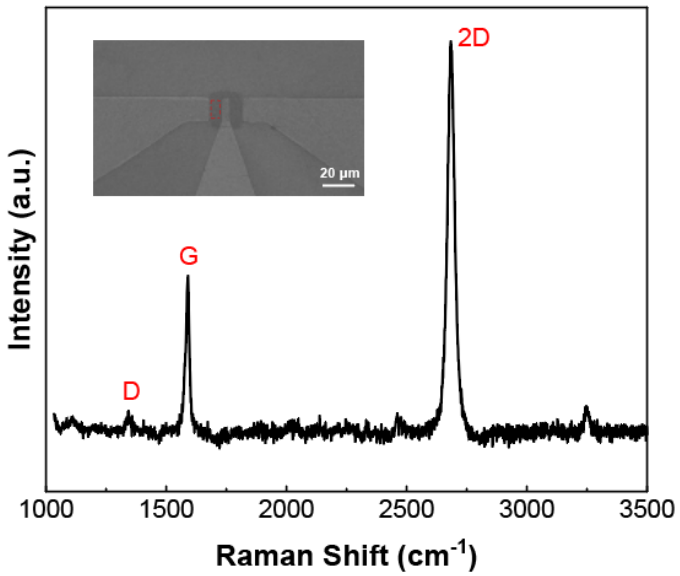

Fig. S1. Raman spectrum acquired from the graphene channel on the left-hand side of the gate (red dashed box in the SEM inset).

To further evaluate the uniformity of the graphene channel, Raman spectroscopy was also performed on the other half of the sensing region, as indicated by the red dashed box in the SEM image (inset of Fig. S1). The corresponding spectrum is shown in Fig. S1. The spectrum exhibits three characteristic peaks at around 1343 cm^{-1}, 1589 cm^{-1} and 2685 cm^{-1}, corresponding to the D, G and 2D bands of graphene, respectively. The D peak is very weak, with an intensity ratio of I_D/I_G = 0.13, while the 2D peak is intense and sharp, giving an I_{2D}/I_G=4.66 and a full width at half maximum of 30.04 cm^{-1}. These Raman parameters are similar to those obtained for the graphene region on the other side of the channel (white dashed box in Fig. 2e), indicating that this region is also high-quality monolayer graphene. Taken together, these results confirm that both sides of the graphene channel consist of uniform, low-defect monolayer graphene.

Theoretical Simulation Methods

The computational system in this study involves NO_2 adsorption on n-doped or p-

doped graphene surfaces, which requires adding or removing charge from the graphene slab. However, calculating the energy of a charged slab using periodic DFT methods is problematic, because the total energy increases linearly with the slab separation in an infinitely repeated charged system, preventing convergence. Therefore, energy corrections are necessary for charged systems in DFT calculations. Previous studies have proposed various solutions [1-5]. In this study, we employed the continuous solvation correction scheme proposed by Andreussi et al. [3], combined with the encounter charge method [5].

The structural optimizations were conducted using the VASP code. The pseudopotentials were described by the GGA-PBE functional, and van der Waals corrections were applied using the DFT-D2 method. During the optimization process, the cutoff energy was set to 450 eV, the Brillouin zone sampling was 3×3×1, the residual force convergence criterion was 0.01 N/Å, and the energy convergence threshold was 10^{-4} eV.

For static self-consistent field calculations and adsorption energy evaluations, the Quantum Espresso package with the Environ plugin was used. The pseudopotentials were described by the GGA-PBE functional, with a wavefunction cutoff of 30 Ry and a charge density cutoff of 240 Ry. The Brillouin zone was sampled using a 5×5×1 k-point mesh, and the energy convergence threshold was 10^{-6} a.u.

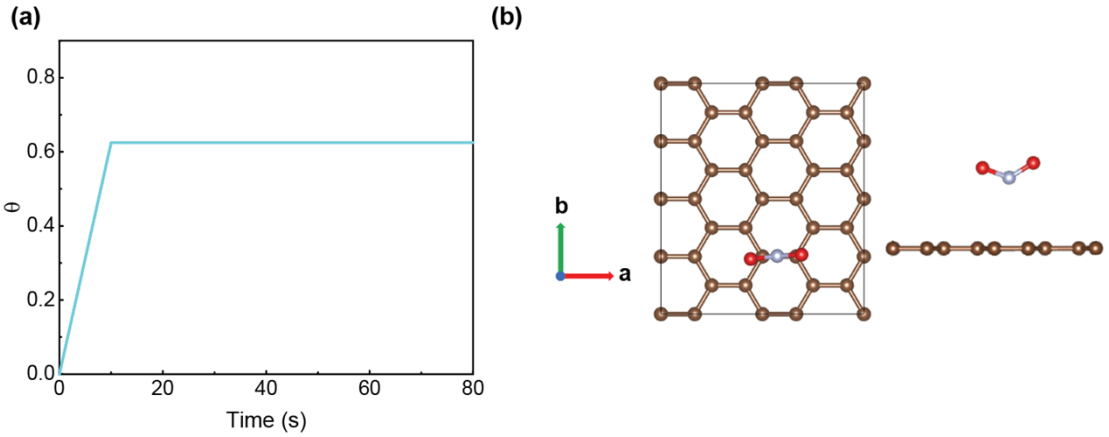

Fig. S2. (a) Adsorption time and adsorption state curve. (b) Structural configuration of monolayer graphene adsorbing NO_2 gas molecules: (left) top view and (right) side view.

Based on the above considerations, a gas adsorption model is established as

follows. Collision theory states that gas molecules must collide with a solid surface to undergo adsorption, meaning that the adsorption rate is proportional to the number of collisions between gas molecules and the unit surface per unit time. According to molecular kinetic theory, the collision frequency n can be expressed as: $n = \frac{P}{\sqrt{2\pi mkT}}$, where P is the partial pressure of the gas phase, m is the molecular mass, k is Boltzmann constant, and T is the temperature.

The adsorption rate is also proportional to the probability of collisions occurring at vacant sites on the surface. Assuming a surface coverage θ, the probability of encountering a vacant site is proportional to the vacancy fraction, $(1-\theta)$. Thus, the adsorption rate can be expressed as:

$$r_a = k_1 \frac{P}{\sqrt{2\pi mkT}}(1-\theta) \tag{1}$$

where k_1 is the proportionality coefficient for adsorption.

In this analysis, the following assumptions are made: (1) Molecules do not interact with each other during the adsorption process; (2) The surface is isotropic; (3) Adsorption on the graphene surface occurs only as a single monolayer.

Due to the weak physical adsorption interaction between NO_2 gas and the graphene surface, the adsorption process is accompanied by desorption. The desorption rate v_d is proportional to the surface coverage θ, and only molecules with kinetic energy greater than the adsorption energy E_a have the probability of desorbing. Thus, the desorption rate can be expressed as:

$$v_d = k_2 e^{\frac{-E_a}{k_B T}} \theta \tag{2}$$

Where k_2 is the proportionality constant for desorption, E_a is the adsorption energy, k_B is Boltzmann constant, and T is the temperature.

Before reaching equilibrium, the adsorption rate v_a exceeds the desorption rate

v_d, resulting in a net reaction rate expressed as $v = v_a - v_d$. To analyze the evolution of adsorption over time, the surface coverage is used to characterize the adsorption state, yielding the following expression:

$$\frac{d\theta}{dt} = k_1 \frac{P}{(2\pi m k_B T)^{1/2}}(1-\theta) - k_2 e^{\frac{-E_a}{k_B T}} \theta \tag{3}$$

Treating terms independent of θ as constants, we define $c_1 = \frac{k_1}{A} \frac{P}{(2\pi m k_B T)^{1/2}}$ and $c_2 = \frac{k_2}{A} e^{\frac{-E_a}{k_B T}}$, simplifying the equation to a first-order differential form:

$$\frac{d\theta}{dt} = c_1(1-\theta) - c_2\,\theta \tag{4}$$

The general solution to this equation is given by:

$$\theta = \frac{C_1}{C_1 + C_2} + \frac{C}{C_1 + C_2} e^{-(C_1 + C_2)t} \tag{5}$$

Using the initial condition $\theta = 0$ at $t = 0$, the constant $c = -c_1$, and the particular solution becomes:

$$\theta = \frac{C_1}{C_1 + C_2} - \frac{C_1}{C_1 + C_2} e^{-(C_1 + C_2)t} \tag{6}$$

At equilibrium $\frac{d\theta}{dt} = 0$, the adsorption and desorption rates are equal $v_a = v_d$, yielding $\theta = \frac{C_1}{C_1 + C_2}$. The relaxation time approaches infinity ($t \to \infty$) at equilibrium. Notably, for any positive parameters c_1 and c_2 *(ensuring* $0 < \frac{C_1}{C_1 + C_2} <$ 1), the function $\theta(t)$ converges monotonically over time to $\frac{C_1}{C_1 + C_2}$. This convergence behavior is consistent with the experimental gas response curves shown in Fig. S2a.

Defining the equilibrium state as $\theta = 0.95 \times \frac{C_1}{C_1 + C_2}$, the relaxation time τ can be expressed as:

$$\tau = -\frac{\ln 0.05}{c_1 + c_2} \approx \frac{3}{c_1 + c_2} \tag{7}$$

The adsorption coefficient c_1 is positively correlated with pressure, which in turn depends on the molecular number density. A higher molecular number density increases collision frequency and pressure. Due to the electron-withdrawing nature of NO_2 molecules, graphene surface charge exerts electrostatic and van der Waals forces, forming a conservative field. Molecules within this field redistribute, with their number density following $n_0 e^{-\frac{\varepsilon}{kT}}$, where ε is the energy in the field. Here, the adsorption energy E_a approximately represents the potential energy near the adsorption site. As c_2 is proportional to $e^{\frac{-E_a}{k_B T}}$, the relaxation time can be rewritten as:

$$\tau = \frac{3}{B_1 \times e^{\frac{E_a}{k_B T}} + B_2 \times e^{\frac{-E_a}{k_B T}}} \tag{8}$$

In typical finite surface systems, the adsorption rate significantly exceeds the desorption rate ($B_1 \gg B_2$). By substituting suitable parameters for B_1 and B_2, the relationship between adsorption energy and relaxation time is shown in Fig. 6a. As the adsorption energy increases, the relaxation time decreases.

As shown in Fig. S2b, in the graphene-NO_2 system, a rectangular graphene supercell containing 32 carbon atoms is selected as the substrate, with its lattice vectors a and b being perpendicular to each other. A vacuum layer of 20 Angstroms is set in the direction of lattice vector c, which is sufficient to shield the periodic interactions. The computational results indicate that the NO_2 molecule is more stable when adsorbed at the bridge site between two adjacent carbon atoms, with the molecule being 3.3 Angstroms away from the graphene surface. This suggests that NO_2 is physically

adsorbed on graphene through van der Waals weak interactions.

To investigate the impact of phosphorus (P) doping and nitrogen (N) doping on the adsorption of NO_2 gas molecules, we study the change in adsorption energy by removing 0.1, 0.2, and 0.3 electrons (P doping) and adding 0.1, 0.2, 0.3, and 0.4 electrons (N doping) on the surface of graphene. The adsorption energy is defined as:

$$E_a = E_{tot} - \left(E_g + E_{NO_2}\right) \tag{9}$$

where E_{tot} is the total energy of the system, E_g is the total energy of graphene, and E_{NO_2} is the energy of the NO_2 molecule. The computational results are shown in Fig. 6b, where the x-axis represents the doping level, with negative values indicating P doping and positive values indicating N doping. The results show that with P doping, the adsorption energy decreases as the doping concentration increases. Conversely, with N doping, the adsorption energy increases as the doping concentration increases.

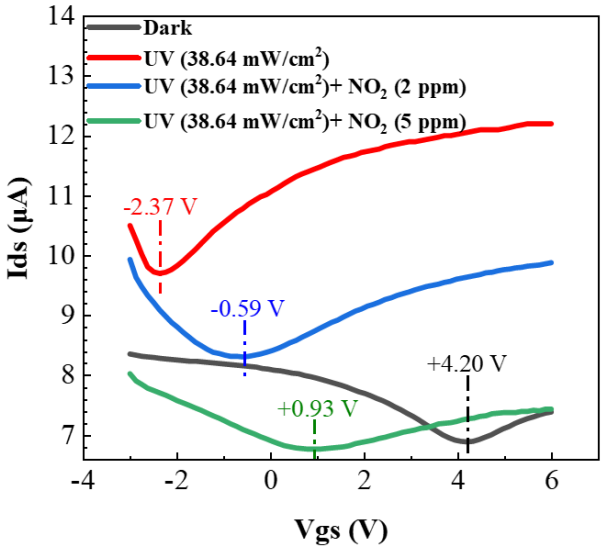

Fig. S3. Transfer characteristics of the sensor under four conditions: no UV, UV illumination, UV + 2 ppm NO_2, and UV + 5 ppm NO_2.

Fig. S3 shows the transfer characteristic curves of the graphene-based gas sensor under four different conditions, measured on a new device in a nitrogen atmosphere at 20–22 °C. Under UV illumination, the transfer curves of the sensor shift from the positive gate voltage direction to the negative gate voltage direction, indicating a transition from p-type to n-type conduction as the charge neutrality point (V_{CNP}) moves

from the positive to the negative region. When 2 ppm NO_2 is introduced, the sensor remains n-type, but the V_{CNP} shifts slightly towards the positive gate voltage region, indicating a weakening of the n-type doping. As the concentration of NO_2 increases to 5 ppm, the V_{CNP} shifts further towards positive gate voltages, crossing zero gate voltage, thus indicating a full reversion to p-type behavior. These results demonstrate the modulation of graphene's semiconductor properties, where UV illumination induces n-type behavior and NO_2 exposure at high concentrations (5 ppm) reverts the graphene back to p-type conduction. This illustrates the combined effects of UV and NO_2 on the electronic structure and doping characteristics of graphene.

References

1. M. Farzalipour Tabriz, B. Aradi, T. Frauenheim and P. Deák, *Comput. Phys. Commun.*, 2019, **240**, 101–105.
2. M. H. Naik and M. Jain, *Comput. Phys. Commun.*, 2018, **226**, 114–126.
3. O. Andreussi, I. Dabo and N. Marzari, *J. Chem. Phys.*, 2012, **136**, 064102.
4. S. Kajita, T. Nakayama and J. Yamauchi, *J. Phys.: Conf. Ser.*, 2006, **29**, 120–123.
5. C. Freysoldt, A. Mishra, M. Ashton and J. Neugebauer, *Phys. Rev. B*, 2020, **102**, 045403.